
Fast and Robust Comparison of Probability Measures in Heterogeneous Spaces

Ryoma Sato^{1,2} Marco Cuturi^{3,4} Makoto Yamada^{1,2,5} Hisashi Kashima^{1,2}

Abstract

The problem of comparing distributions endowed with their own geometry appears in various settings, e.g., when comparing graphs, high-dimensional point clouds, shapes, and generative models. Although the Gromov Wasserstein (GW) distance is usually presented as the natural geometry to handle such comparisons, computing it involves solving a NP-hard problem. In this paper, we propose the Anchor Energy (AE) and Anchor Wasserstein (AW) distances, simpler alternatives to GW built upon the representation of each point in each distribution as the 1D distribution of its distances to all other points. We propose a sweep line algorithm to compute AE *exactly* in $O(n^2 \log n)$ time, where n is the size of each measure, compared to a naive implementation of AE requires $O(n^3)$ efforts. This is quasi-linear w.r.t. the description of the problem itself. AW can be pending a single $O(n^3)$ effort, in addition to the $O(n^2)$ cost of running the Sinkhorn algorithm. We also propose robust versions of AE and AW using rank-based criteria rather than cost values. We show in our experiments that the AE and AW distances perform well in 3D shape comparison and graph matching, at a fraction of the computational cost of popular GW approximations.

1. Introduction

Wasserstein distances have proved useful to compare two probability distributions when they are both supported on the *same* metric space. This is exemplified by its several applications, notably in image (Ni et al., 2009; Rabin et al., 2011; De Goes et al., 2012; Schmitz et al., 2018) or natural language processing (Kusner et al., 2015; Rolet et al., 2016), biology (Schiebinger et al., 2019), or when training generative models (Arjovsky et al., 2017; Salimans et al.,

2018; Genevay et al., 2018; De Goes et al., 2012). Yet, when these two distributions live in a two *different* and seemingly unrelated spaces, simple Wasserstein distances fail and one must resort to the more involved framework of Gromov-Wasserstein (GW) distances (Mémoli, 2011).

The generality of GW. The GW distance replaces the linear objective appearing in optimal transport (OT) with a quadratic function of the transportation plan that quantifies some form of metric distortion when transporting points from one space to another. GW is not only an elegant answer to this problem, it is also well grounded in theory (Sturm, 2012) and has been successfully applied to shape matching (Mémoli, 2007; Solomon et al., 2016), machine translation (Alvarez-Melis & Jaakkola, 2018; Grave et al., 2019), or graph matching (Xu et al., 2019b;a). The GW distance can compare two distributions supported on spaces, in which the support of these measures itself is endowed with a metric, or more generally a cost structure. This pair of distributional and metric information is called a *measured metric spaces* (MMS), which reduces, in a discrete setting to a probability vector of size n paired with a $n \times n$ cost matrix.

GW approximations. Although well grounded in theory, the GW geometry is not a convenient computational object: its exact computation requires solving a NP-hard quadratic assignment problem (QAP) (Mémoli, 2007). Therefore, many approximations of GW have been considered. Aflalo et al. (2015) relaxed the problem into a convex quadratic program, while Kezurer et al. (2015) relaxed it as a semidefinite program. Although tractable for small n , these relaxations have scalability issues that prevent their use beyond a few hundred points. Solomon et al. (2016) and Peyré et al. (2016) proposed to modify the QAP using entropic regularization. When comparing two MMS supported on n points, this results in an algorithm that alternates between a local linearization of the GW objective (requiring two matrix multiplications at a $2n^3$ cost) followed by Sinkhorn iterations (for a $O(n^2)$ cost). While this approach is currently favored by the community to approximate GW, it is usually too costly for large n and can suffer from numerical instability due to the fact that the scale of the cost matrix can change at each linearization, making the Sinkhorn kernel numerically unstable. To bring down computational costs further, Vayer et al. (2019) proposed

¹Kyoto University ²RIKEN AIP ³CREST-ENSAE ⁴Google Brain ⁵JST PRESTO. Correspondence to: Ryoma Sato <r.sato@ml.ist.i.kyoto-u.ac.jp>.

to restrict the GW problem to measures supported on Euclidean spaces, and to generalize the slicing approach of Rabin et al. (2011) to obtain a cheaper $O(n \log n)$ computational price, pending additional efforts to rotate/register point clouds. Despite its cheaper price tag, these restrictions cannot handle non-Euclidean data or costs (graphs, geodesic distances of shapes, and more general arbitrary kernels and costs) and can therefore only be of use for a small fraction of the application fields now in need of a scalable GW approximation.

Contributions. We propose in this work simple alternatives to the GW approach built on the idea that two points living in different MMSs can be compared using a common feature representation: that feature representation consists in representing each point of a MMS as the 1D distribution of all its distances/costs to all other points in its MMS. This feature representation was introduced in the computer graphics and computer vision fields to compare 3D shapes (Osada et al., 2002; Hamza & Krim, 2003; Gelfand et al., 2005; Manay et al., 2006), and allows us to compare two points independently of where they initially lie, by simply comparing these two distributions of costs in $\mathcal{P}(\mathbb{R})$. As a result, two MMSs can be represented as two distributions on $\mathcal{P}(\mathbb{R})$, namely cast as elements of $\mathcal{P}(\mathcal{P}(\mathbb{R}))$. Our paper focuses in particular on the energy distance (Székely & Rizzo, 2013; Sejdinovic et al., 2013) derived from these distributions of anchor distributions, where we use the Wasserstein distance itself as a negative definite kernel to compare two elements in $\mathcal{P}(\mathbb{R})$ (Wasserstein distance are indeed n.d. in $\mathcal{P}(\mathbb{R})$ as remarked by Kolouri et al. (2016)). We call this approach the Anchor Energy (AE) distance, and one of the main contributions of this paper is to propose an efficient approach to compute it in $O(n^2 \log n)$ time, resulting in a *quasi-linear* complexity w.r.t the input size (a MMS is described with a n^2 cost matrix). The AE distance is therefore, as far as we know, the fastest non-trivial approach to compare two distributions supported on different spaces. We also consider the entropic regularized Wasserstein distance of the distributions of anchor 1D distributions, using here again the Wasserstein distance as the ground metric. We call this variant the Anchor Wasserstein (AW) distance. In experiments, we show that the AE and AW distances improve on entropic GW in 3D shape comparison and graph matching tasks, while being order of magnitudes faster and applicable to scales not seen before in the literature.

2. Background

We call a *measured metric space* (MMS) any measure μ on a measurable space \mathcal{X} endowed with a cost function $\mathcal{X} \times \mathcal{X} \rightarrow \mathbb{R}$. Equivalently, a discrete measured metric set (MMSet) of size n is a pair $S = (\mathbf{a}, \mathbf{C}) \in \Sigma_n \times \mathbb{R}^{n \times n}$,

where, for a given $n \geq 1$, $\Sigma_n = \{\mathbf{a} \in \mathbb{R}_+^n \mid \sum_i \mathbf{a}_i = 1\}$ is the n -probability simplex. Intuitively a MMSet is a probability vector \mathbf{a} , putting mass on elements that are exclusively described in terms of a $n \times n$ cost matrix \mathbf{C} . Such pairs of weights/cost matrices typically arise when describing the points of a point cloud, along with the shortest path distance matrix on that cloud, induced from a graph, or more generally any other cost function (Solomon et al., 2016; Peyré et al., 2016). Note that, unlike the sliced Gromov-Wasserstein (SGW) distance recently proposed by Vayer et al. (2019), we assume no knowledge on the points that constitute a MMSet, and only work from \mathbf{C} (the SGW framework assumes that \mathbf{C} is a squared-Euclidean distance matrix). Before describing the GW distance between two MMSETS, we review the standard Wasserstein distance and quadratic assignments.

2.1. Wasserstein Distance

Given two measurable spaces \mathcal{X} and \mathcal{Y} , a cost function $c : \mathcal{X} \times \mathcal{Y} \rightarrow \mathbb{R}$, and two measures $\mu \in \mathcal{P}(\mathcal{X})$ and $\nu \in \mathcal{P}(\mathcal{Y})$, the optimal transport problem between μ and ν can be written as

$$\text{OT}(\mu, \nu) = \min_{\gamma \in \Pi(\mu, \nu)} \mathbb{E}_{(X, Y) \sim \gamma} [c(X, Y)],$$

where $\Pi(\mu, \nu)$ is the set of joint couplings on $\mathcal{X} \times \mathcal{Y}$ that have marginals μ, ν . When $\mathcal{X} = \mathcal{Y}$ and the cost c is a metric on \mathcal{X} raised to the power p (with $p \geq 1$), the optimum $\text{OT}(\mu, \nu)^{1/p}$ is called the p -Wasserstein metric between μ, ν . We consider next two subcases that are relevant for the remainder of this paper.

Discrete formulation. When $\mathbf{a}^1, \mathbf{a}^2 \in \Sigma_n$, a cost matrix $\mathbf{C} \in \mathbb{R}^{n \times n}$ suffices to instantiate the OT problem:

$$\text{OT}(\mathbf{a}^1, \mathbf{a}^2) = \min_{\mathbf{P} \in U(\mathbf{a}^1, \mathbf{a}^2)} \sum_{ij} \mathbf{P}_{ij} \mathbf{C}_{ij}, \quad \text{where}$$

$$U(\mathbf{a}^1, \mathbf{a}^2) = \{\mathbf{P} \in \mathbb{R}_+^{n \times m} \mid \mathbf{P} \mathbb{1}_m = \mathbf{a}^1, \mathbf{P}^\top \mathbb{1}_n = \mathbf{a}^2\}$$

is the transportation polytope and $\mathbb{1}_m$ the m -vector of ones.

Univariate case. When $\mu, \nu \in \mathcal{P}(\mathbb{R})$, and $c(x, y) = |x - y|^p$, $p \geq 1$, one has that (Santambrogio, 2015, §2)

$$\text{OT}_p(\mu, \nu) = \int_0^1 |H_\mu^{-1}(u) - H_\nu^{-1}(u)|^p du,$$

where H_μ is the empirical or cumulant density function of measure μ and therefore H_μ^{-1} its quantile function. We will write in that case $W_p = (\text{OT}_p)^{1/p}$ for the p -Wasserstein distance. Note further that for $p = 1$ one recovers

$$\text{OT}_p(\mu, \nu) = \int_{-\infty}^{\infty} |H_\mu(u) - H_\nu(u)| du.$$

2.2. Gromov Wasserstein Distance

The Gromov Wasserstein (GW) problem between two MMS (μ, c_1), (ν, c_2) is defined as follows:

$$\text{GW}(\mu, \nu) = \min_{\gamma \in \Pi(\mu, \nu)} \mathbb{E}_{(X, Y), (X', Y') \sim \gamma} (c_1(X, Y) - c_2(X', Y'))^2.$$

When instantiated on two MMSETS, $S^1 = (\mathbf{a}^1, \mathbf{C}^1)$ and $S^2 = (\mathbf{a}^2, \mathbf{C}^2)$, this problem reduces to

$$\text{GW}(S^1, S^2) = \min_{\mathbf{P} \in U(\mathbf{a}^1, \mathbf{a}^2)} \sum_{ijkl} \mathbf{P}_{ik} \mathbf{P}_{jl} |\mathbf{C}_{ij}^1 - \mathbf{C}_{kl}^2|^2. \quad (1)$$

As recalled in §1, the GW distance has found success in several applications, such as shape matching, machine translation, and graph matching. However, computing it is NP-hard (Mémoli, 2007), and even simply evaluating it knowing the optimal γ beforehand would have a $O(n^3)$ computational pricetag (Vayer et al., 2019).

2.3. Slicing Approach

As mentioned above, the Wasserstein distance between two univariate distributions (namely when $\mathbf{C}_{ij} = |x_i - x_j|$ for values $x_i \in \mathbb{R}$) can be solved by computing cumulative distribution functions (CDFs), and therefore only requires sorting real values with a $O(n \log n)$ time complexity (Rabin et al., 2011). The sliced Wasserstein distance (Rabin et al., 2011) leverages this feature by projecting measures onto random 1-dimensional lines, to sum up these Wasserstein distances. Recently, Vayer et al. (2019) proposed a sliced Gromov Wasserstein (SGW) distance that exploits this idea more generally when comparing two distributions lying in two Euclidean spaces. To be efficient, this method requires an additional “realignment” step which computes a linear transform of one of the input measures. The SGW approach assumes that both MMSETS are embedded in \mathbb{R}^d , and can only consider Euclidean geometry. That method cannot, therefore, be generalized to more generic families of costs. In this paper, we do exploit the fast computation of 1D Wasserstein distances as Vayer et al. (2019) did, but without relying on a projection step.

3. Anchor Distances for MMSETS

3.1. Points as Anchors

To compare two MMSETS, we map each point from each MMSet to the distribution of its (weighted) ground cost or distance to all other points within that MMSet. This idea was successfully used in the computer graphics field (Gelfand et al., 2005; Mémoli, 2011) under the name of *local distribution of distances*, spanning several successful approaches for 3D shape comparison. Fig. 1 summarizes this idea. Specifically, the cost distribution from the anchor

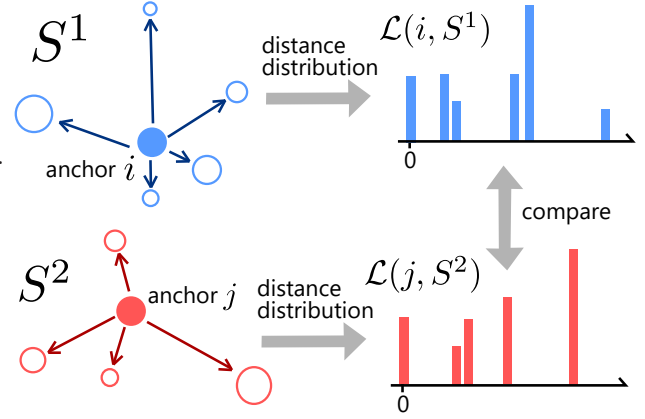


Figure 1. Local distributions of distances of two MMSETS.

indexed by i within $S = (\mathbf{a}, \mathbf{C})$ is simply the 1D empirical distribution of the cost of line i in \mathbf{C} , weighted by \mathbf{a} ,

$$\mathcal{L}(i, \mathbf{a}, \mathbf{C}) := \sum_{j=1}^n \mathbf{a}_j \delta_{\mathbf{C}_{ij}} \in \mathcal{P}(\mathbb{R}),$$

where for $x \in \mathbb{R}$, δ_x is the Dirac mass at x . Notice that this can be interpreted, for continuous measures, as the push-forward $(c(x, \cdot))_{\#} \mu$ for an anchor $x \in \mathcal{X}$. We represent a MMSet as a distribution of local distributions of distances

$$\mathcal{A}(\mathbf{a}, \mathbf{C}) := \sum_{i=1}^n \mathbf{a}_i \delta_{\mathcal{L}(i, \mathbf{a}, \mathbf{C})} \in \mathcal{P}(\mathcal{P}(\mathbb{R})),$$

which we call the anchor feature representation of a MMSet. Although the anchor feature map is not injective (Mémoli, 2011) (i.e., there exists two MMSETS $S^1 \neq S^2$ such that $\mathcal{A}(S^1) = \mathcal{A}(S^2)$), many powerful features for 3D shape comparison such as the (global) distribution of distances (Osada et al., 2002) and eccentricity (Hamza & Krim, 2003; Manay et al., 2006) can be computed from the anchor feature of a 3D shape. Moreover, it is proved that almost all point clouds can be reconstructed from the (global) distribution of distances (Boutin & Kemper, 2004), therefore from the anchor feature.

In some applications, however, scales of MMSETS may differ. Yet, the anchor feature is not robust to scaling. Namely, $\mathcal{A}(\mathbf{a}, \mathbf{C}) \neq \mathcal{A}(\mathbf{a}, \lambda \mathbf{C})$ for some $\lambda \neq 1$. This issue is a common one when using GW distances. Although dividing the distance by the largest value in the distance matrix can alleviate this problem, if anomaly points, noise, or clutters are contained in the MMSETS, for example due to the scanning process of 3D shapes, it is difficult to settle this problem. To overcome this issue, we propose a robust variant of the anchor feature. Instead of using matrix \mathbf{C} directly, we preprocess it to output its rank-based statistics, or, put differently, we turn each entry in the matrix into its empirical distribution function, or yet more simply into its rank divided by n^2 . This translates into rank-based anchor feature

distributions defined as:

$$\begin{aligned} p(i, j, \mathbf{C}) &:= \frac{1}{n^2} \#\{(k, l) \mid \mathbf{C}_{kl} \leq \mathbf{C}_{ij}\} \in [0, 1], \\ \mathcal{L}_R(i, \mathbf{a}, \mathbf{C}) &:= \sum_{j=1}^n \mathbf{a}_j \delta_{p(i, j, \mathbf{C})} \in \mathcal{P}([0, 1]), \\ \mathcal{A}_R(\mathbf{a}, \mathbf{C}) &:= \sum_{i=1}^n \mathbf{a}_i \delta_{\mathcal{L}_R(i, \mathbf{a}, \mathbf{C})} \in \mathcal{P}(\mathcal{P}([0, 1])), \end{aligned}$$

where $\#$ denotes the number of elements in the set. In the experiments, we show that the distances using robust anchor feature performs better than the distances using normal anchor features when the scales of the entries in cost matrices of MMSets differ significantly.

3.2. Anchor Energy

In this paper, we propose two distances using the anchor feature. The first variant is energy distance with the one-dimensional Wasserstein kernel. Specifically,

$$\begin{aligned} \text{AE}_p(S^1, S^2) &:= 2\mathbb{E}_{h^1 \sim \mathcal{A}(S^1), h^2 \sim \mathcal{A}(S^2)}[\text{OT}_p^p(h^1, h^2)] \\ &\quad - \mathbb{E}_{h_1^1, h_2^1 \sim \mathcal{A}(S^1)}[\text{OT}_p^p(h_1^1, h_2^1)] \\ &\quad - \mathbb{E}_{h_1^2, h_2^2 \sim \mathcal{A}(S^2)}[\text{OT}_p^p(h_1^2, h_2^2)]. \end{aligned} \quad (2)$$

The robust version AE_R is defined by replacing the anchor feature \mathcal{A} with the robust anchor feature \mathcal{A}_R . Since turning a measure into a quantile function is a feature map onto a Hilbert space of functions, OT_1 and OT_2^2 are conditionally negative definite (Kolouri et al., 2016). Therefore, AE_p is a valid energy distance for $p = 1, 2$ (Sejdinovic et al., 2013), and provides a metric structure to the anchor feature space. Especially, $\text{AE}_p(S^1, S^2) = 0$ if and only if $\mathcal{A}(S^1) = \mathcal{A}(S^2)$, and the triangle inequality holds. It should be noted that this is not a metric in the original MMSets space because the anchor feature is not injective (Mémoli, 2011). However, this provides nonetheless powerful discriminative power because subclass of anchor features are shown to be powerful in the computer vision field (Osada et al., 2002; Hamza & Krim, 2003; Manay et al., 2006), and almost all point clouds can be reconstructed from the anchor feature (Boutin & Kemper, 2004).

Each term of Eq. 2 can be explicitly expressed as follows:

$$\begin{aligned} &\mathbb{E}_{h^1 \sim \mathcal{A}(S^1), h^2 \sim \mathcal{A}(S^2)}[\text{OT}_p^p(h^1, h^2)] \\ &= \sum_{ij} \mathbf{a}_i^1 \mathbf{a}_j^2 \text{OT}_p^p(h^1, h^2) \\ &= \sum_{ij} \mathbf{a}_i^1 \mathbf{a}_j^2 \min_{\mathbf{P} \in U(\mathbf{a}^1 \mathbf{a}^2)} \sum_{kl} \mathbf{P}_{kl} |\mathbf{C}_{ik}^1 - \mathbf{C}_{jl}^2|^p. \end{aligned} \quad (3)$$

The last representation looks similar to the GW distance (Eq.1), but the AE distance calculates an average of the local optimal transports of all pairs of points, whereas the GW distance computes a global optimal transport. Since computing an optimal transport of sorted one-dimensional distribution takes linear time, *the AE distance requires cubic time when computed naively*. We propose an efficient algorithm to compute the AE distance in $O((n^2 + m^2) \log(nm))$ time in §3.4.

3.3. Anchor Energy Matching

A strong appeal of OT and GW based distances is that they also provide assignments. We propose the anchor energy matching, a simple assignment based on the anchor energy (Eq.3), by the following formula:

$$\text{AEM} = \sum_{ij} \mathbf{a}_i^1 \mathbf{a}_j^2 \operatorname{argmin}_{\mathbf{P} \in U(\mathbf{a}^1 \mathbf{a}^2)} \sum_{kl} \mathbf{P}_{kl} |\mathbf{C}_{ik}^1 - \mathbf{C}_{jl}^2|^p.$$

This assignment takes an average of the local optimal transports of all pairs of points as the anchor energy distance, whereas the assignment by the GW distance computes a global optimal transport. Therefore, AEM cannot distinguish detailed structure or take interactions between points into consideration, but the AEM can provide robust assignment that preserves the role of points. For example, suppose there exists an outlier point in a MMSet. The GW assignment is influenced by this outlier point. In contrast, a small fraction of local optimal transports are affected by this outlier, and affected transportation plans do not take too large values because all transportation plans must be doubly-stochastic. Therefore, transportation plans of inlier points are dominant terms, and the outlier point does not affect the AEM much. We confirm that AEM can provide a good assignment that preserves roles of nodes in networks in the experiment section (§4.4).

Time Complexity: AEM can be computed in $O(nm(n + m) + n^2 \log n + m^2 \log m)$ time, and a matching vector for a single node can be computed in $O(nm \log(nm) + m^2 \log m)$ by the naive computation.

3.4. Sweep Line Anchor Energy

We propose in this section an efficient computation algorithm for the AE distance, named Sweep Line Anchor Energy (SLAE). This computes the AE distance in $O((n^2 + m^2) \log(nm))$ time for any integer $p \geq 1$. We introduce the case of $p = 1$ for simplicity, but the idea can be naturally extended to general integers p . This method can be applied to the robust anchor energy just by replacing the cost matrix with normalized ranks. SLAE utilizes a technique inspired from the sweep line algorithm (Shamos & Hoey,

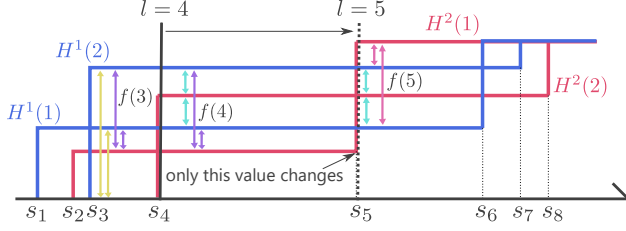


Figure 2. Overview of SLAE: The AE distance is the integration of the total variations $f(l)$ of the CDFs. SLAE sums up the total variations $f(1), f(2), \dots, f(n^2 + m^2 - 1)$ sweeping a vertical line from left to right. The key idea is only terms that involve a single CDF change in each segment, and these total variations can be managed efficiently by balanced trees.

1976; Fortune, 1987), which was originally proposed in the computational geometry field. Figure 2 illustrates the algorithm behind SLAE.

Intuitive Explanation: The AE distance requires at least cubic time if the optimal transport values are computed separately because the AE distance involves nm optimal transport values, and each optimal transport value takes at least a linear time to be computed. Instead, SLAE computes the summation of all optimal transport values at once. The Wasserstein-1 distance of one-dimensional distributions is equal to the area between the CDFs of the distributions. We have n red CDFs from the first distribution and m blue CDFs from the second distribution. The AE distance is the sum of areas between all pairs of red functions and blue functions. SLAE integrates these areas from left to right at once, rather than computes each area separately. This change of viewpoint is important but does not improve the computational complexity solely. Another important insight is that each CDF is piecewise constant, and the CDF of $\mathcal{L}(i, \mathbf{a}, \mathbf{C})$ changes only at $\mathbf{C}_{i1}, \mathbf{C}_{i2}, \dots, \mathbf{C}_{in}$, which makes $(n^2 + m^2)$ change points in total. We assume all change points are unique without loss of generality. SLAE cuts the real number line at these change points, which makes $(n^2 + m^2 - 1)$ segments. In each segment, all CDFs are constant. Thus, the sum of the areas in each segment is the total variation of red and blue CDFs times the length of the segment. SLAE accumulates areas between the CDFs for these segments from left to right. In addition to that, adjacent segments are almost same but only one CDF changes. Although a change of one CDF makes differences involving linear number of terms, efficient data structures, such as B-tree and Fenwick tree, offer a logarithmic time algorithm to compute the partial summation. In total, there are $(n^2 + m^2 - 1)$ segments, and it takes logarithmic time to update the total variation in each segment, the time complexity of SLAE is quasi-quadratic w.r.t. n and m .

We explain the algorithm of SLAE and prove its validity formally. Let $(i_l, j_l, k_l) \in \{1, \dots, n\} \times \{1, \dots, m\} \times \{1, 2\}$ ($l = 1, 2, \dots, n^2 + m^2$) be indices such that

$\mathbf{C}_{i_l j_l}^{k_l} \leq \mathbf{C}_{i_{l+1} j_{l+1}}^{k_{l+1}} \leq \dots \leq \mathbf{C}_{i_{n^2+m^2} j_{n^2+m^2}}^{k_{n^2+m^2}}$, and $(i_l, j_l, k_l) \neq (i_{l'}, j_{l'}, k_{l'})$ for $l \neq l'$. Let $s_l = \mathbf{C}_{i_l j_l}^{k_l}$ ($l = 1, \dots, n^2 + m^2$), and let $H^k(i, x)$ be the CDF of $\mathcal{L}(i, \mathbf{a}^k, \mathbf{C}^k)$. Then,

Proposition 1.

$$\mathbb{E}_{h^1 \sim \mathcal{A}(S^1), h^2 \sim \mathcal{A}(S^2)} [OT_1(h^1, h^2)] = \sum_{l=1}^{n^2+m^2-1} (s_{l+1} - s_l) f(l),$$

where $f(l)$ is the total variation:

$$f(l) = \sum_{i=1}^n \sum_{j=1}^m \mathbf{a}_i^1 \mathbf{a}_j^2 |H^1(i, s_l) - H^2(j, s_l)|.$$

The key idea of SLAE is in each iteration l , only $H^{k_l}(i_l)$ changes (i.e., $H^k(i, s_{l+1}) = H^k(i, s_l)$ for $i \neq i_l$ or $k \neq k_l$). Let $\mathcal{S}^k(u, v)$ and $\mathcal{T}^k(u, v)$ be

$$\begin{aligned} \mathcal{S}_l^k(u, v) &= \sum_{i: u \leq H^k(i, s_l) < v} \mathbf{a}_i^k, \\ \mathcal{T}_l^k(u, v) &= \sum_{i: u \leq H^k(i, s_l) < v} \mathbf{a}_i^k H^k(i, s_l). \end{aligned}$$

Proposition 2.

$$\begin{aligned} f(l) &= f(l-1) - \mathbf{a}_{i_l}^{k_l} (\mathcal{S}_l^{k_l'}(-\infty, c) \cdot c - \mathcal{T}_l^{k_l'}(-\infty, c)) \\ &\quad - \mathbf{a}_{i_l}^{k_l} (\mathcal{T}_l^{k_l'}(c, \infty) - \mathcal{S}_l^{k_l'}(c, \infty) \cdot c) \\ &\quad + \mathbf{a}_{i_l}^{k_l'} (\mathcal{S}_{l+1}^{k_l'}(-\infty, c') \cdot c' - \mathcal{T}_{l+1}^{k_l'}(-\infty, c')) \\ &\quad + \mathbf{a}_{i_l}^{k_l'} (\mathcal{T}_{l+1}^{k_l'}(c', \infty) - \mathcal{S}_{l+1}^{k_l'}(c', \infty) \cdot c'), \end{aligned}$$

where $c = H^{k_l}(i_l, s_l)$ and $c' = H^{k_l'}(i_l, s_{l+1})$, and k_l' is the opposite index of k_l (i.e., $k_l' = 2$ if $k_l = 1$ and $k_l' = 1$ if $k_l = 2$). ∞ denotes a sufficiently large constant such as the largest absolute value in the cost matrices.

We utilize balanced trees such as the B-tree (Bayer & McCreight, 1972) and Fenwick tree (Fenwick, 1994) to compute \mathcal{S}^k and \mathcal{T}^k . A balanced tree T maintains an array and can calculate the following operations in $O(\log n)$ time, where n is the number of elements in the array.

- $\text{Add}(T, i, x)$: Add x to T_i ,
- $T(u, v)$: Calculate $\sum_{i: u \leq i \leq v} T_i$.

Note that an index i is not necessarily an integer but a real value in general. The update of f in Proposition 2 requires $O(n + m)$ time naively because \mathcal{S}^k and \mathcal{T}^k involve $O(n + m)$ terms. This summation can be sped up to $O(\log(nm))$ time by balanced trees. The pseudo code of SLAE is shown in Algorithm 3.4.

Algorithm 1 Sweep Line Anchor Energy

```

 $W \leftarrow 0, f[0] \leftarrow 0$ 
 $H[0][i] \leftarrow 0 \ (i = 0, \dots, n)$ 
 $H[1][j] \leftarrow 0 \ (j = 0, \dots, m)$ 
 $t[i \cdot n + j] \leftarrow (\mathbf{C}_{ij}^1, i, j, 1, 2) \ (i, j = 1, \dots, n)$ 
 $t[n^2 + i \cdot n + j] \leftarrow (\mathbf{C}_{ij}^2, i, j, 2, 1) \ (i, j = 1, \dots, m)$ 
 $(s_l, i_l, j_l, k_l, k'_l) \leftarrow \text{sorted}(t)[l] \ (l = 1, \dots, n^2 + m^2)$ 
Initialize  $\mathcal{S}^1, \mathcal{S}^2, \mathcal{T}^1$ , and  $\mathcal{T}^2$  to 0
for  $l = 1, \dots, n^2 + m^2 - 1$  do
     $c \leftarrow H[k_l][i_l]$ 
     $f[l] \leftarrow f[l - 1]$ 
     $f[l] \leftarrow f[l] - \mathbf{a}_{i_l}^{k_l} \cdot (\mathcal{S}^{k'_l}(-\infty, c) \cdot c - \mathcal{T}^{k'_l}(-\infty, c))$ 
     $f[l] \leftarrow f[l] - \mathbf{a}_{i_l}^{k_l} (\mathcal{T}^{k'_l}(c, \infty) - \mathcal{S}^{k'_l}(c, \infty) \cdot c)$ 
    Add( $\mathcal{S}^{k_l}, H[k_l][i_l], -\mathbf{a}_{i_l}^{k_l}$ )
    Add( $\mathcal{T}^{k_l}, H[k_l][i_l], -\mathbf{a}_{i_l}^{k_l} H[k_l][i_l]$ )
     $H[k_l][i_l] \leftarrow H[k_l][i_l] + \mathbf{a}_{j_l}^{k_l}$ 
    Add( $\mathcal{S}^{k_l}, H[k_l][i_l], \mathbf{a}_{i_l}^{k_l}$ )
    Add( $\mathcal{T}^{k_l}, H[k_l][i_l], \mathbf{a}_{i_l}^{k_l} H[k_l][i_l]$ )
     $c' \leftarrow H[k_l][i_l]$ 
     $f[l] \leftarrow f[l] + \mathbf{a}_{i_l}^{k_l} \cdot (\mathcal{S}^{k'_l}(-\infty, c') \cdot c' - \mathcal{T}^{k'_l}(-\infty, c'))$ 
     $f[l] \leftarrow f[l] + \mathbf{a}_{i_l}^{k_l} (\mathcal{T}^{k'_l}(c', \infty) - \mathcal{S}^{k'_l}(c', \infty) \cdot c')$ 
     $W \leftarrow W + (s_{l+1} - s_l) \cdot f[l]$ 
end
return  $W$ 

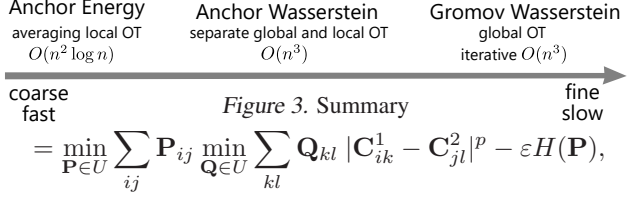
```

Time Complexity: We analyze the complexity of SLAE briefly. The sorting of $\{s_i\}_{i=1, \dots, n^2+m^2}$ requires $O((n^2 + m^2) \log(nm))$ time. The loop iterates $n^2 + m^2 - 1$ times. In each iteration, there are a constant number of updates and queries for \mathcal{T}_i and \mathcal{S}_i . If we use balanced trees as the data structures for \mathcal{T}_i and \mathcal{S}_i , each query and update requires $O(\log(nm))$ times. Therefore, the total time complexity is $O((n^2 + m^2) \log(nm))$.

3.5. OT between Anchors: Anchor Wasserstein

We introduce the second distance using the anchor feature. This is the entropic-regularized Wasserstein distance using the Wasserstein distance as the ground metric. Using Wasserstein distance as the ground metric of the Wasserstein distance have been proved to be powerful to exploit the underground hierarchical structure (Yurochkin et al., 2019; Dukler et al., 2019). We use the hierarchical Wasserstein distance to compare two anchor features. Specifically, the Anchor Wasserstein (AW) distance is defined as follows:

$$\begin{aligned}
 AW_p(\mathcal{S}^1, \mathcal{S}^2) &:= OT(\mathcal{A}(\mathcal{S}^1), \mathcal{A}(\mathcal{S}^2)) \\
 &= \min_{\mathbf{P} \in U(\mathbf{a}^1, \mathbf{a}^2)} \sum_{ij} \mathbf{P}_{ij} OT_p^p(\mathcal{L}_i^1, \mathcal{L}_j^2) - \varepsilon H(\mathbf{P})
 \end{aligned}$$



where $U = U(\mathbf{a}^1, \mathbf{a}^2)$ is the set of transportation plans, $\mathcal{L}_i^k = \mathcal{L}(i, \mathbf{a}^k, \mathbf{C}^k)$ is the local distribution of distances, $H(\mathbf{P}) = -\sum_{ij} \mathbf{P}_{ij} (\log \mathbf{P}_{ij} - 1)$ is the entropy, and $\varepsilon > 0$ is the regularization coefficient. This formula is also similar to the GW distance (Eq. 1) as the AE distance, but the AW optimizes global and local assignments separately. In the case of $\varepsilon = 0$, this is equal to the lower bound of the GW distance introduced in Mémoli (2011), and this is also a lower bound of the AE distance because the AE distance uses the marginalized transportation, which is in the set U of transportation plans. However, $\varepsilon = 0$ requires more computational cost by solving a liner programming (Mémoli, 2011). Thanks to the entropic regularization, the Sinkhorn algorithm (Cuturi, 2013) can speed up the computation. Namely, the cost matrix $\mathbf{C}_{ij} = OT_p^p(\mathcal{L}_i^1, \mathcal{L}_j^2)$ can be computed in $O(nm(n+m))$ time, and the optimal transport \mathbf{P}^* can be computed in quadratic time by the Sinkhorn algorithm. The total time complexity is cubic, but this computes the cost matrix only once, whereas the GW distance computes cost matrix iteratively.

The AW distance can take more detailed structure compared to the AE distance because the AW distance optimizes the global assignment, whereas the AE distance uses the marginalized transportation as the global assignment. Figure 3 summarizes three methods to compare two probabilistic measures in heterogeneous spaces.

4. Experiments

We experimentally assess the performance of the AE and AW distances by answering the following questions. (Q1) **Scalability:** How fast are the linear sweep algorithm (SLAE) compared to a naive implementation of AE? (Q2) **Shape Comparison:** Are the AE and AW distances useful for 3D shape comparison? (Q3) **Robustness:** Are robust versions of the AE and AW distances robust against scaling and noise? (Q4) **Matching:** Does the anchor energy matching preserve the role of nodes? (Q5) **Barycenter:** Do AE and AW barycenters provide good summaries of datasets from different domains? We use the Sinkhorn algorithm for the GW distance with entropic regularization (Solomon et al., 2016) as a baseline method (denoted by GW). We run the Sinkhorn algorithm in the log space for numerical stability. The experimental details are provided in the supplementary materials.

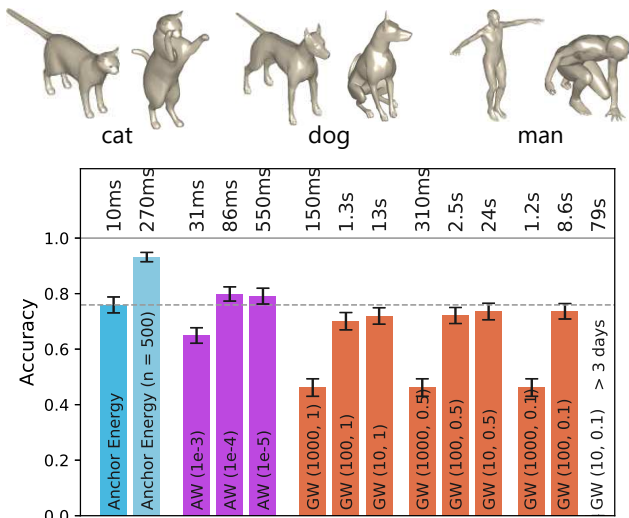


Figure 5. **3D Shape Comparison:** (Top) Examples of 3D shapes. (Bottom) Accuracy of 1-NN classification using each distance. $AW(\varepsilon)$ means the AW distance with regularization coefficient ε . $GW(\varepsilon, \tau)$ means the GW distance with regularization coefficient ε and learning rate τ . Note that the scales of ε in the AW and GW distances are different.

4.1. Scalability (Q1)

We assess the scalability of our linear sweep approaches. For $n = 32, 64, \dots, 2048$, we sample n points from 3D cat shapes illustrated in Figure 5 (Top). In this experiment, the cost functions are the geodesic distances in the original shape, and distributions are uniform. We compute the AE distance using the naive triple loop method and SLAE with only a *single* core of CPU, which is desirable to compute many pairs of shapes parallelly. We also compute the AW distance and GW distance for illustrative purposes, since they do not compute the same thing. Figure 4 gives orders of magnitudes to execute each method, highlighting the quasi-quadratic complexity of SLAE.

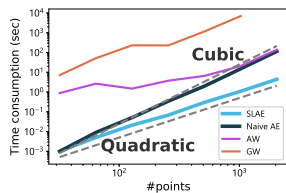


Figure 4. Scalability.

4.2. Shape Comparison (Q2)

We apply the AE and AW distance to the 3D shape data. We use the non-rigid world dataset (Bronstein et al., 2006) which contains 148 3D shapes of 12 classes. We exclude the “shark” class because it contains only one shape. Figure 5 (Top) shows examples of 3D shapes. We use the uniform weights and the geodesic distances on 3D shapes as the cost function. Each 3D shape involves approximately 3000 vertices. We randomly sample $n = 100$ vertices to make the GW distance feasible, although the SLAW algorithm works efficiently even for larger shapes. $148 \cdot 147/2 = 10878$ pairs of shapes are compared in total. We randomly sample

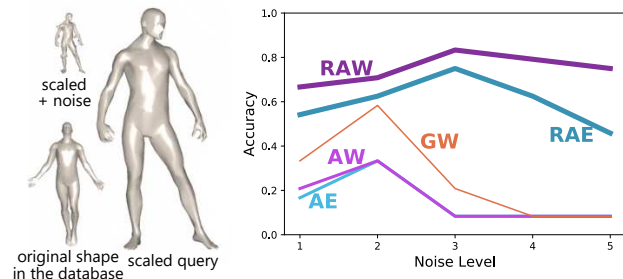


Figure 6. **Robust 3D shape comparison:** (Left) Examples of original shapes in the database and scaled, and scaled + noisy queries. (Right) Accuracy of 1-NN classification using each distance.

80 percent of all the shapes as the training data set, and we conduct leave-one-out 1-NN classification for each training data set 100 times. Figure 5 (Bottom) shows accuracy and average speed to compare a single pair of shapes for each distance, which also reports the accuracy of the AE distance with $n = 500$ points for illustrative purposes. This indicates that the AE distance performs comparably to the AW and GW distance even though the AE distance works fast and has no hyperparameters. This result suggests that the AE distance is a handy metric for shape comparison, especially when there are too few samples to choose hyperparameters appropriately.

4.3. Robustness (Q3)

We apply the robust versions of the AE and AW distances to the SHREC10 robustness benchmark (Bronstein et al., 2010). This dataset contains shapes in the database and transformed query shapes for each shape. We use scaling transformation queries and scaling + noise transformation queries in this experiment. Each noised query has the noise level from 1 to 5. We use the normal and robust versions of the AE and AW distances to retrieve a shape in the database corresponding to the query shape by the nearest neighbor retrieval. We use the training data, which contain 12 shapes and 120 query shapes, for evaluation since no training phase is involved in our classifier. Figure 6 (Right) reports the accuracy for each noise level, which also reports the accuracy of the GW distance as a reference record. This indicates that robust versions of the AE and AW distances can handle the difference of scaling, whereas normal distances suffer from drop of accuracy as the noise level increases.

4.4. Matching (Q4)

In this experiment we generate a pair of graphs using the Barabasi-Albert model (Barabasi & Albert, 1999), which is known to be useful to model scale-free networks, such as social networks and computer networks, and compute a matching from the nodes of one graph to the nodes of

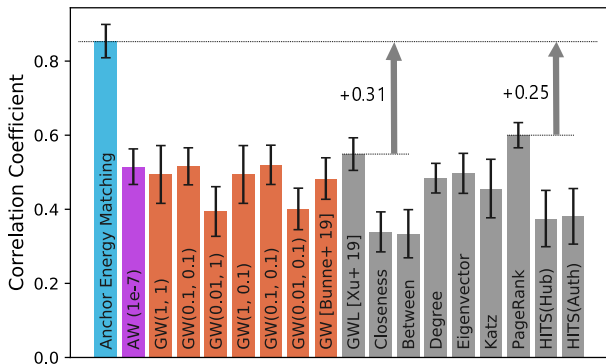
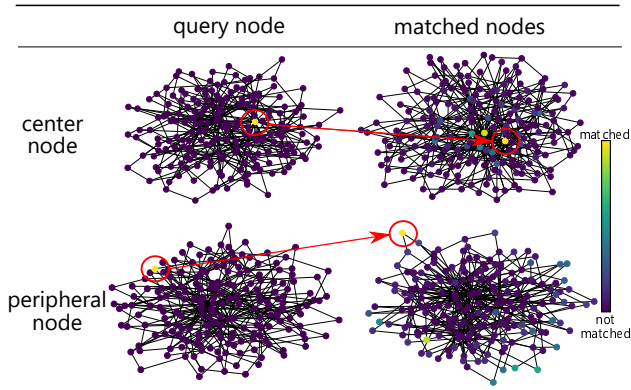


Figure 7. **Node Matching:** (Top) Yellow nodes in the right graphs indicate the nodes are matched, and the dark-blue nodes in the right graphs indicate the nodes are not matched. This shows the center node matches with the center nodes and the peripheral node matches with the peripheral nodes. (Bottom) Correlation coefficients.

the other graph, and compute the correlation coefficient between the indexes of matched nodes. The smaller the indexes of nodes are, the more central roles the nodes tend to play in the Barabasi-Albert model. Therefore, if a matching matches the nodes that play similar roles, the correlation coefficients becomes high. We compute the Anchor Energy matching, the Gromov Wasserstein matching, and the optimal global assignment P^* of the AW distance. We use an open implementation (Bunne et al., 2019) to tune hyperparameters for the GW matching in addition to various hyperparameters. We also compare these matchings with the Gromov Wasserstein Learning (Xu et al., 2019b), which is a state-of-the-art graph matching method using the GW distance. We also use matching methods based on various centrality measures including PageRank (Brin & Page, 1998) and HITS (Kleinberg, 1999). These methods match nodes in the order of these centrality measures. Figure 7 (Top) shows examples of the AE matching of two graphs generated by the Barabasi-Albert model. It shows that the center node matches with center nodes in the other network and the peripheral node matches with peripheral nodes in the other network. Figure 7 (Bottom) reports the average correlation coefficients of ten pairs of graphs. This result indicates that the AE matching preserves roles of nodes better than the other methods. The GW and AW matching fail this task because they keenly fit noise signals whereas the AE matching is robust to noise thanks to averaging transportation plans. It should be noted that this task is more difficult than that in (Xu et al., 2019b) because we match different graphs generated by the same process, whereas Xu et al. (2019b) matched a graph with the same graph with noise.

4.5. Barycenter (Q5)

We compute barycenters of 3D shapes generated from MNIST handwritten digits dataset (LeCun et al., 1998) into 2-dimensional Euclidean space with respect to the AE and AW geometries. These shapes are rotated in 3-dimensional spaces, and lying in a different space from barycenters, which makes it difficult to summarize these data. The AE and AW distances can be applied to these settings since they can compare measures lying in different spaces. We optimize the sum of AE and AW distances from the data shapes by gradient descent. The gradients are computed by an auto-gradient package PyTorch (Paszke et al., 2019). Figure 8 shows the data and barycenters. The AE barycenter fails to provide good summaries of digits 2 and 3, whereas the AW barycenters preserve characteristics of all digits thanks to more precise global matching.

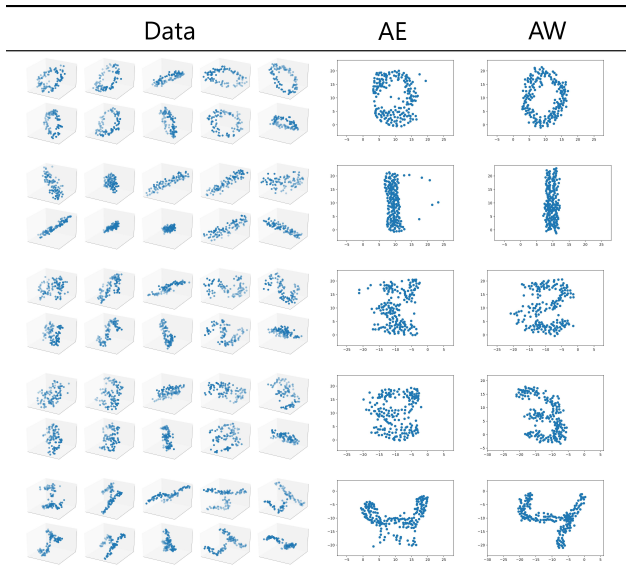


Figure 8. **Barycenters of 3D digits:** Barycenters of 3D digits in 2-dimensional Euclidean space w.r.t. the AE and AW geometries.

5. Conclusion

We introduced in this paper the Anchor Energy (AE) distance and Anchor Wasserstein (AW) distance, novel dissimilarity measures for two measured metric sets lying in heterogeneous spaces. They first extract the Anchor Features of both measures to represent these measures, which are originally lying in different spaces, in the same space. The AE distance is the energy distance and AW distance is the entropic-regularized Wasserstein distance of the anchor features. We proposed an exact algorithm to compute the AE distance exactly in $O((n^2 + m^2) \log(nm))$ time, shaving a linear term w.r.t a naive implementation. We also proposed the AE matching, a novel assignment method inspired by the AE distance. We experimentally showed that our sweeping line approach scales quasi-quadratically w.r.t. the size of the support, and it is faster than other OT-based metrics. We also showed that our proposed methods perform well in the shape comparison and network matching.

5.1. Acknowledgments

This work was supported by JSPS KAKENHI Grant-Number 15H01704 and the JST PRESTO program JP-MJPR165A.

References

- Aflalo, Y., Bronstein, A., and Kimmel, R. On convex relaxation of graph isomorphism. *Proceedings of the National Academy of Sciences*, 112(10):2942–2947, 2015.
- Alvarez-Melis, D. and Jaakkola, T. S. Gromov-wasserstein alignment of word embedding spaces. In *Proceedings of the 2018 Conference on Empirical Methods in Natural Language Processing, EMNLP*, pp. 1881–1890, 2018.
- Arjovsky, M., Chintala, S., and Bottou, L. Wasserstein generative adversarial networks. In *Proceedings of the 34th International Conference on Machine Learning, ICML*, pp. 214–223, 2017.
- Barabasi, A.-L. and Albert, R. Emergence of scaling in random networks. *Science*, 286(5439):509–512, 1999.
- Bayer, R. and McCreight, E. M. Organization and maintenance of large ordered indices. *Acta Inf.*, 1:173–189, 1972.
- Boutin, M. and Kemper, G. On reconstructing n -point configurations from the distribution of distances or areas. *Adv. Appl. Math.*, 32(4):709–735, 2004.
- Brin, S. and Page, L. The anatomy of a large-scale hyper-textual web search engine. *Computer Networks*, 30(1-7): 107–117, 1998.
- Bronstein, A. M., Bronstein, M. M., and Kimmel, R. Efficient computation of isometry-invariant distances between surfaces. *SIAM J. Scientific Computing*, 28(5): 1812–1836, 2006.
- Bronstein, A. M., Bronstein, M. M., Castellani, U., Falcidieno, B., Fusiello, A., Godil, A., Guibas, L. J., Kokkinos, I., Lian, Z., Ovsjanikov, M., Patanè, G., Spagnuolo, M., and Toldo, R. Shrec’10 track: Robust shape retrieval. In *Eurographics Workshop on 3D Object Retrieval*, pp. 71–78, 2010.
- Bunne, C., Alvarez-Melis, D., Krause, A., and Jegelka, S. Learning generative models across incomparable spaces. In *Proceedings of the 36th International Conference on Machine Learning, ICML*, pp. 851–861, 2019.
- Cuturi, M. Sinkhorn distances: Lightspeed computation of optimal transport. In *Advances in Neural Information Processing Systems 26: Annual Conference on Neural Information Processing Systems 2013, NIPS*, pp. 2292–2300, 2013.
- De Goes, F., Breeden, K., Ostromoukhov, V., and Desbrun, M. Blue noise through optimal transport. *ACM Transactions on Graphics (TOG)*, 31(6):1–11, 2012.
- Dukler, Y., Li, W., Lin, A. T., and Montúfar, G. Wasserstein of wasserstein loss for learning generative models. In *Proceedings of the 36th International Conference on Machine Learning, ICML*, pp. 1716–1725, 2019.
- Fenwick, P. M. A new data structure for cumulative frequency tables. *Softw., Pract. Exper.*, 24(3):327–336, 1994.
- Fortune, S. A sweepline algorithm for voronoi diagrams. *Algorithmica*, 2(1-4):153, 1987.
- Gelfand, N., Mitra, N. J., Guibas, L. J., and Pottmann, H. Robust global registration. In *Third Eurographics Symposium on Geometry Processing*, pp. 197–206, 2005.
- Genevay, A., Peyré, G., and Cuturi, M. Learning generative models with sinkhorn divergences. In *Proceedings of the 21st International Conference on Artificial Intelligence and Statistics, AISTATS*, pp. 1608–1617, 2018.
- Grave, E., Joulin, A., and Berthet, Q. Unsupervised alignment of embeddings with wasserstein procrustes. In *Proceedings of the 22nd International Conference on Artificial Intelligence and Statistics, AISTATS*, pp. 1880–1890, 2019.
- Hamza, A. B. and Krim, H. Geodesic object representation and recognition. In *Discrete Geometry for Computer Imagery, 11th International Conference, DGCI*, pp. 378–387, 2003.

- Kezurer, I., Kovalsky, S. Z., Basri, R., and Lipman, Y. Tight relaxation of quadratic matching. *Comput. Graph. Forum*, 34(5):115–128, 2015.
- Kleinberg, J. M. Authoritative sources in a hyperlinked environment. *J. ACM*, 46(5):604–632, 1999.
- Kolouri, S., Zou, Y., and Rohde, G. K. Sliced wasserstein kernels for probability distributions. In *Proceedings of the IEEE Conference on Computer Vision and Pattern Recognition*, pp. 5258–5267, 2016.
- Kusner, M., Sun, Y., Kolkin, N., and Weinberger, K. From word embeddings to document distances. In *Proceedings of the 32nd International Conference on Machine Learning, ICML*, pp. 957–966, 2015.
- LeCun, Y., Bottou, L., Bengio, Y., and Haffner, P. Gradient-based learning applied to document recognition. *Proceedings of the IEEE*, 86(11):2278–2324, 1998.
- Manay, S., Cremers, D., Hong, B., Yezzi, A. J., and Soatto, S. Integral invariants for shape matching. *IEEE Trans. Pattern Anal. Mach. Intell.*, 28(10):1602–1618, 2006.
- Mémoli, F. On the use of gromov-hausdorff distances for shape comparison. In *Proceedings of the Symposium on Point Based Graphics*, pp. 81–90, 2007.
- Mémoli, F. Gromov–Wasserstein distances and the metric approach to object matching. *Foundations of Computational Mathematics*, 11(4):417–487, 2011.
- Ni, K., Bresson, X., Chan, T. F., and Esedoglu, S. Local histogram based segmentation using the wasserstein distance. *International Journal of Computer Vision*, 84(1): 97–111, 2009.
- Osada, R., Funkhouser, T. A., Chazelle, B., and Dobkin, D. P. Shape distributions. *ACM Trans. Graph.*, 21(4): 807–832, 2002.
- Paszke, A., Gross, S., Massa, F., Lerer, A., Bradbury, J., Chanan, G., Killeen, T., Lin, Z., Gimelshein, N., Antiga, L., Desmaison, A., Köpf, A., Yang, E., DeVito, Z., Raison, M., Tejani, A., Chilamkurthy, S., Steiner, B., Fang, L., Bai, J., and Chintala, S. Pytorch: An imperative style, high-performance deep learning library. In *Advances in Neural Information Processing Systems 32: Annual Conference on Neural Information Processing Systems 2019, NeurIPS*, pp. 8024–8035, 2019.
- Peyré, G., Cuturi, M., and Solomon, J. Gromov-wasserstein averaging of kernel and distance matrices. In *Proceedings of the 33rd International Conference on Machine Learning, ICML*, pp. 2664–2672, 2016.
- Rabin, J., Peyré, G., Delon, J., and Bernot, M. Wasserstein barycenter and its application to texture mixing. In *Proceedings of Scale Space and Variational Methods in Computer Vision*, pp. 435–446, 2011.
- Rolet, A., Cuturi, M., and Peyré, G. Fast dictionary learning with a smoothed wasserstein loss. In *Artificial Intelligence and Statistics*, pp. 630–638, 2016.
- Salimans, T., Zhang, H., Radford, A., and Metaxas, D. Improving GANs using optimal transport. In *Proceedings of the Sixth International Conference on Learning Representations, ICLR*, 2018.
- Santambrogio, F. *Optimal transport for applied mathematicians*. Birkhauser, 2015.
- Schiebinger, G., Shu, J., Tabaka, M., Cleary, B., Subramanian, V., Solomon, A., Gould, J., Liu, S., Lin, S., Berube, P., et al. Optimal-transport analysis of single-cell gene expression identifies developmental trajectories in reprogramming. *Cell*, 176(4):928–943, 2019.
- Schmitz, M. A., Heitz, M., Bonneel, N., Ngole, F., Coeurjolly, D., Cuturi, M., Peyré, G., and Starck, J.-L. Wasserstein dictionary learning: Optimal transport-based unsupervised nonlinear dictionary learning. *SIAM Journal on Imaging Sciences*, 11(1):643–678, 2018.
- Sejdinovic, D., Sriperumbudur, B., Gretton, A., Fukumizu, K., et al. Equivalence of distance-based and rkhs-based statistics in hypothesis testing. *The Annals of Statistics*, 41(5):2263–2291, 2013.
- Shamos, M. I. and Hoey, D. Geometric intersection problems. In *Proceedings of the 17th Annual Symposium on Foundations of Computer Science, FOCS*, pp. 208–215, 1976.
- Solomon, J., Peyré, G., Kim, V. G., and Sra, S. Entropic metric alignment for correspondence problems. *ACM Trans. Graph.*, 35(4):72:1–72:13, 2016.
- Sturm, K.-T. The space of spaces: curvature bounds and gradient flows on the space of metric measure spaces. *arXiv preprint arXiv:1208.0434*, 2012.
- Székely, G. J. and Rizzo, M. L. Energy statistics: A class of statistics based on distances. *Journal of statistical planning and inference*, 143(8):1249–1272, 2013.
- Vayer, T., Flamary, R., Tavenard, R., Chapel, L., and Courty, N. Sliced gromov-wasserstein. In *Advances in Neural Information Processing Systems 32: Annual Conference on Neural Information Processing Systems 2019, NeurIPS*, 2019.

Xu, H., Luo, D., and Carin, L. Scalable gromov-wasserstein learning for graph partitioning and matching. In *Advances in Neural Information Processing Systems 32: Annual Conference on Neural Information Processing Systems 2019, NeurIPS 2019*, pp. 3046–3056, 2019a.

Xu, H., Luo, D., Zha, H., and Carin, L. Gromov-wasserstein learning for graph matching and node embedding. In *Proceedings of the 36th International Conference on Machine Learning, ICML*, pp. 6932–6941, 2019b.

Yurochkin, M., Claici, S., Chien, E., Mirzazadeh, F., and Solomon, J. M. Hierarchical optimal transport for document representation. In *Advances in Neural Information Processing Systems 32: Annual Conference on Neural Information Processing Systems 2019, NeurIPS*, pp. 1599–1609, 2019.

A. Experimental Details

We use the Fenwick trees (Fenwick, 1994) for the implementation of \mathcal{S}^k and \mathcal{T}^k . The Sinkhorn algorithm for the AW distance and the inner loop of the GW distance stops when the relative change in the transportation plan becomes less than 10^{-6} . The outer loop of the GW distance (Solomon et al., 2016) stops when the relative change in the transportation plan or the objective value is less than 10^{-6} . We measure speeds of algorithms with a single core of Intel Xeon CPU E7-4830.

A.1. Scalability (Q1)

We first compute the geodesic distance matrices \mathbf{D}^1 and \mathbf{D}^2 of the two cat shapes. For $n = 32, 64, \dots, 2048$, we sample n points uniformly randomly for each shape and sample the corresponding rows and columns of the distance matrix to make the sampled distance matrix \mathbf{C}_n^1 and $\mathbf{C}_n^2 \in \mathbb{R}_+^{n \times n}$. We compute the AE, AW, and GW distance of \mathbf{C}_n^1 and \mathbf{C}_n^2 with the uniform distribution. We do not include the time consumption of preprocessing (i.e., the distance calculation and sampling) in the result. We set $\varepsilon = 10^{-5}$ for the AW distance, and $\varepsilon = 10$ and $\tau = 1$ for the GW distance.

A.2. Shape Comparison (Q2)

We first compute the geodesic distance matrix for each shape. For each shape, we then sample $n = 100$ points uniformly randomly and sample the corresponding rows and columns of the distance matrix to make the sampled distance matrix $\mathbf{C} \in \mathbb{R}_+^{n \times n}$. We compute the AE, AW, and GW distance of each pair of sampled distance matrices with uniform distribution. We parallelly compute distances using a large-scale computer cluster. The time consumption is the average time to compute the distance of a pair of shapes with a single core of Intel Xeon CPU E7-4830 for 100 random pairs since the time consumption on the shared computer cluster is affected by external causes. Then, we compute the accuracy and standard deviation by the following procedure: For 100 times, (1) we sample $k = 118$ shapes $\{S_1, S_2, \dots, S_k\}$ from all the shapes, (2) for each $i = 1, 2, \dots, k$, we classify shape S_i by the nearest neighbor in $\{S_1, S_2, \dots, S_{i-1}, S_{i+1}, \dots, S_k\}$, and (3) we report the number of shapes that are classified to the true label.

A.3. Robustness (Q3)

We set $\varepsilon = 10^{-6}$ for the AW distance, $\varepsilon = 10^{-8}$ for the robust AW distance, and $\varepsilon = 100$ and $\tau = 1$ for the GW distance.

A.4. Matching (Q4)

We use the Barabasi Albert model with $n = 200$ nodes and $m = 2$ attachments in this experiment.

A.5. Barycenter (Q5)

We generate 3D point clouds of digits from MNIST handwritten digits dataset (LeCun et al., 1998) by the following process: (1) we sample 100 points $\{\mathbf{p}_i\}_{i=1, \dots, 100}$ in the 2-dimensional lattice $\{1, 2, \dots, 28\} \times \{1, 2, \dots, 28\}$ with a probability proportional to the brightness of that pixel, (2) we sample a random 3-dimensional rotation matrix \mathbf{M} uniformly, (3) we rotate points $\{\mathbf{p}_i\}$ by \mathbf{M} , and (4) we add a i.i.d. Gaussian noise $\mathcal{N}(\mathbf{0}, 0.25\mathbf{I})$ to each point. We generate 10 point clouds for each digit.

B. Proofs

Proof of Proposition 1. Since $H^k(i, x)$ is a piecewise-constant function,

$$\begin{aligned}
 & \mathbb{E}_{h^1 \sim \mathcal{A}(S^1), h^2 \sim \mathcal{A}(S^2)} [\text{OT}_p^p(h^1, h^2)] \\
 &= \sum_{i=1}^n \sum_{j=1}^m \mathbf{a}_i^1 \mathbf{a}_j^2 \text{OT}_p^p(\mathcal{L}(i, \mathbf{a}^1, \mathbf{C}^1), \mathcal{L}(j, \mathbf{a}^2, \mathbf{C}^2)) \\
 &= \sum_{i=1}^n \sum_{j=1}^m \mathbf{a}_i^{(1)} \mathbf{a}_j^{(2)} \int_0^\infty |H^1(i, x) - H^2(j, x)| dx \\
 &= \sum_{i=1}^n \sum_{j=1}^m \mathbf{a}_i^{(1)} \mathbf{a}_j^{(2)} \sum_{l=1}^{K-1} (s_{l+1} - s_l) |H^1(i, s_l) - H^2(j, s_l)|
 \end{aligned}$$

$$\begin{aligned}
 &= \sum_{l=1}^{K-1} (s_{l+1} - s_l) \sum_{i=1}^n \sum_{j=1}^m \mathbf{a}_i^{(1)} \mathbf{a}_j^{(2)} |H^1(i, s_l) - H^2(j, s_l)| \\
 &= \sum_{l=1}^{K-1} (s_{l+1} - s_l) f(l).
 \end{aligned}$$

□

Proof of Proposition 2. We assume $n_1 = n_2 = n$ without loss of generality by appropriately zero-padding \mathbf{a}^1 and \mathbf{a}^2 .

$$\begin{aligned}
 &f(l+1) - f(l) \\
 &= - \left(\mathbf{a}_{i_l}^{k_l} \sum_{x=1}^n \mathbf{a}_x^{k'_l} |H^{k_l}(i_l, s_l) - H^{k'_l}(x, s_l)| \right) \\
 &\quad + \left(\mathbf{a}_{i_l}^{k_l} \sum_{x=1}^n \mathbf{a}_x^{k'_l} |H^{k_l}(i_l, s_{l+1}) - H^{k'_l}(x, s_{l+1})| \right) \\
 &= - \left(\mathbf{a}_{i_l}^{k_l} \sum_{x=1}^n \mathbf{a}_x^{k'_l} |c - H^{k'_l}(x, s_l)| \right) \\
 &\quad + \left(\mathbf{a}_{i_l}^{k_l} \sum_{x=1}^n \mathbf{a}_x^{k'_l} |c' - H^{k'_l}(x, s_{l+1})| \right) \\
 &= - \left(\mathbf{a}_{i_l}^{k_l} \sum_{x: H^{k'_l}(x, s_l) < c} \mathbf{a}_x^{k_l} c - \mathbf{a}_x^{k_l} H^{k'_l}(x, s_l) \right) \\
 &\quad - \left(\mathbf{a}_{i_l}^{k_l} \sum_{x: c < H^{k'_l}(x, s_l)} \mathbf{a}_x^{k_l} H^{k'_l}(x, s_l) - \mathbf{a}_x^{k_l} c \right) \\
 &\quad + \left(\mathbf{a}_{i_l}^{k_l} \sum_{x: H^{k'_l}(x, s_{l+1}) < c'} \mathbf{a}_x^{k_l} c - \mathbf{a}_x^{k_l} H^{k'_l}(x, s_{l+1}) \right) \\
 &\quad + \left(\mathbf{a}_{i_l}^{k_l} \sum_{x: c' < H^{k'_l}(x, s_{l+1})} \mathbf{a}_x^{k_l} H^{k'_l}(x, s_{l+1}) - \mathbf{a}_x^{k_l} c' \right) \\
 &= -\mathbf{a}_{i_l}^{k_l} (\mathcal{S}_l^{k'}(-\infty, c)c - \mathcal{T}_l^{k'}(-\infty, c)) \\
 &\quad - \mathbf{a}_{i_l}^{k_l} (\mathcal{T}_l^{k'}(c, \infty) - \mathcal{S}_l^{k'}(c, \infty)c) \\
 &\quad + \mathbf{a}_{i_l}^{k_l} (\mathcal{S}_l^{k'}(-\infty, c')c' - \mathcal{T}_l^{k'}(-\infty, c')) \\
 &\quad + \mathbf{a}_{i_l}^{k_l} (\mathcal{T}_l^{k'}(c', \infty) - \mathcal{S}_l^{k'}(c', \infty)c')
 \end{aligned}$$

□